HHS Public Access

Author manuscript

J Am Chem Soc. Author manuscript; available in PMC 2024 August 09.

Published in final edited form as:

J Am Chem Soc. 2023 August 09; 145(31): 17143–17150. doi:10.1021/jacs.3c03812.

Single-Molecular Dissection of Liquid−Liquid Phase Transitions

Pravin Pokhrel[†],
Department of Chemistry and Biochemistry, Kent State University, Kent, Ohio 44242, United States

Sagun Jonchhe[†],
Department of Chemistry and Biochemistry, Kent State University, Kent, Ohio 44242, United States

Wei Pan,
Department of Chemistry and Biochemistry, Kent State University, Kent, Ohio 44242, United States

Hanbin Mao
Department of Chemistry and Biochemistry, Kent State University, Kent, Ohio 44242, United States

Abstract

Interaction between peptides and nucleic acids is a ubiquitous process that drives many cellular functions, such as replications, transcriptions, and translations. Recently, this interaction has been found in liquid−liquid phase separation (LLPS), a process responsible for the formation of newly discovered membraneless organelles with a variety of biological functions inside cells. In this work, we studied the molecular interaction between the poly-L-lysine (PLL) peptide and nucleic acids during the early stage of an LLPS process at the single-molecule level using optical tweezers. By monitoring the mechanical tension of individual nucleic acid templates upon PLL addition, we revealed a multistage LLPS process mediated by the long-range interactions between nucleic acids and polyelectrolytes. By varying different types (ssDNA, ssRNA, and dsDNA) and sequences (A-, T-, G-, or U-rich) of nucleic acids, we pieced together transition diagrams of the PLL−nucleic acid condensates from which we concluded that the propensity to form rigid nucleic acid−PLL complexes reduces the condensate formation during the LLPS process. We anticipate that these results are instrumental in understanding the transition mechanism of LLPS

Corresponding Author: Hanbin Mao − Department of Chemistry and Biochemistry, Kent State University, Kent, Ohio 44242, United States; hmao@kent.edu.
[†]These authors P.P. and S.J. contributed equally.

Supporting Information

The Supporting Information is available free of charge at https://pubs.acs.org/doi/10.1021/jacs.3c03812.
Materials, list of oligos, microfluidic chamber, preparation of nanopipets, microfluidic chamber for the nanopipet assay, synthesis of RCA constructs, synthesis of RNA RCT constructs, synthesis of poly(dA/dT) dsDNA template, optical tweezers setup to study the LLPS of nucleic acids and PLL, conjugation of antidig antibody on polystyrene beads, in vitro phase separation assay of all nucleic acid templates under study, fusion time of nucleic acid−PLL droplets, summary of nucleic acid/PLL phase transition, persistence length (P) and contour length (L) measurement, all nucleic acid molecules and their FX curves at different concentrations of PLL, and References (PDF)

Complete contact information is available at: https://pubs.acs.org/10.1021/jacs.3c03812

The authors declare no competing financial interest.

condensates, which allows new strategies to interfere with the biological functions of LLPS condensates inside cells.

Graphical Abstract

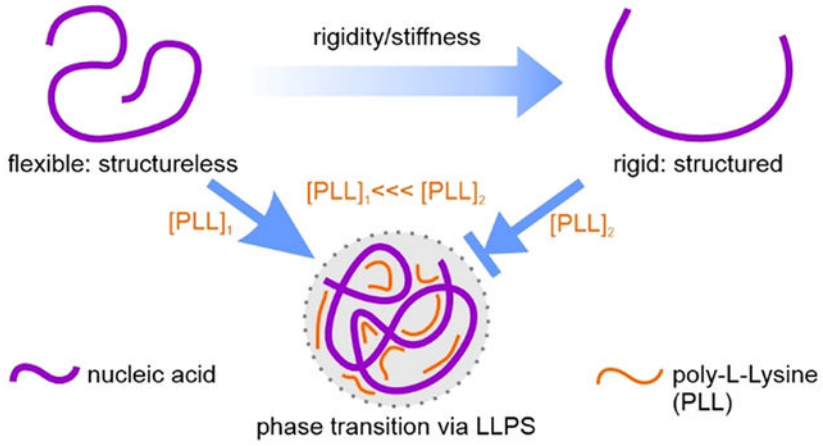

INTRODUCTION

Recently, membraneless compartments, also known as biomolecular condensates, have been found inside cells. These compartments are formed by the liquid−liquid phase separation (LLPS) process,[1,2] which results in condensates made of macromolecules such as proteins and nucleic acids. Since the condensates are not bounded by membranes, they have shown dynamic properties with their components freely exchangeable with cytoplasmic contents, a feature not present in cell organelles.

Many biological activities[3,4] such as DNA organization and processing,[5–9] cellular signaling,[10,11] and immune response[12,13] can be modulated by macromolecular condensates. The major components in these condensates are either standalone proteins or protein−nucleic acid mixtures that are prone to LLPS. Many examples have shown that the interactions between DNA and proteins lead to the condensate formation via the LLPS process.[5,6,14–16] RNAs also demonstrate similar roles in the LLPS process by interacting with cationic amino acids in proteins.[17–22] Methods such as turbidity and fluorescence measurements exist to investigate the LLPS process at the ensemble average level. Simple microscopy techniques have also been used to study LLPS events; however, they could not reveal phase separations below threshold concentrations of the participating components. The high sensitivity in single-molecule techniques[23–26] allows us to probe the LLPS process from the intramolecular perspective on a particular component under a much wider concentration range unreachable by bulk techniques. This feature permits a simplified profiling on the LLPS process since intermolecular interactions for the specific component can be excluded. Among single-molecular studies, few investigations focus on the LLPS condensates from a mechanical perspective.[23–28] Given that LLPS condensates partake in many mechanobiological processes such as chromosomal segregation during cell

division[29,30] and transportation inside cells,[31,32] it becomes an urgent call to evaluate the condensates from mechanical aspects.

In this work, we investigated the interaction between an exemplary cationic peptide, poly-L-lysine (PLL), and DNA/RNA molecules during the formation of the condensates from a mechanical perspective using optical tweezers in a microfluidic setting. The superior sensitivity of optical tweezers in the tension measurement of a single-molecule nucleic acid template also allowed us to scrutinize the sequence and structure effects of nucleic acids on the condensate formation. To this end, we used polydeoxyadenosine (poly(dA)) single-stranded DNA (ssDNA), polydeoxythymidine (poly(dT)) ssDNA, poly(dA/dT) duplex DNA, polyribouridine (poly(rU)) single-stranded RNA (ssRNA), and polyriboadenosine (poly(rA)) ssRNA as templates upon which condensation processes initiated by PLL are followed by observing the variation of tensile force in individual templates. We revealed four distinct phases characterized by different molecular interactions between the nucleic acids and PLL during condensate formation. After summarizing these distinct behaviors in a phase transition diagram with different concentrations of PLL, we ascribed different phase behaviors to the stiffness of the nucleic acid−PLL complexes, which is determined by the secondary structures formed in each nucleic acid template. Such a hypothesis was verified by a poly-G-quadruplex (a DNA secondary structure) containing ssDNA template, which started to form LLPS condensates only under high PLL concentrations. This key finding indicates preferential LLPS/condensate formation among certain types of nucleic acids, which can be utilized to design molecules to interfere with these important biological processes.

EXPERIMENTAL SECTION

Single-Molecule Optical Tweezer Experiments.

All the single-molecule nucleic acid templates were studied in a custom-built dualtrap optical tweezer instrument,[33] which is described in SI Section S9. The two laser foci were used to trap two polystyrene beads (diameters: 1.76 and 2.32 μm) coated with streptavidin and antidigoxigenin antibody, respectively. Streptavidin-coated polystyrene beads were purchased ready-to-use, whereas antidigoxigenin antibody-coated polystyrene beads were prepared in lab (see SI Section S10). A single-molecule nucleic acid template was tethered between the two beads via biotin−streptavidin and digoxigenin (dig)/antidig linkages. Tension was applied to the tethered template by moving the two beads apart using a steerable mirror that controls one of the laser foci. The tension was calculated based on the spring constant of each trap and the displacement of the beads from the center of the trap.[33] The force vs extension (FX) profile (0–65 pN) of the templates was recorded using a LabView program (National Instruments) at a 1 kHz frequency and a loading rate of 5.5 pN/s (10–30 pN range).

To study the condensation of peptide−nucleic acid templates, a four-channel microfluidic chamber was used, as described in SI Section S3. In brief, the streptavidin-coated beads conjugated with the nucleic acid template and the antidig-coated beads were flowed separately from the bottommost and topmost channels to the two middle channels via microcapillary tubes (see Figures S1 and S2). Two different beads were then captured

separately by the two laser traps in a 10 mM tris buffer (pH 7.4) supplemented with 100 mM KCl. To study the condensation of nucleic acid and PLL, the FX profile of a single-molecule nucleic acid template was first recorded in the buffer without PLL (lower middle channel) and then escorted to the buffer containing PLL (upper middle channel).

Synthesis of Single-Molecule ssDNA Constructs.

The ssDNA templates were synthesized by the rolling cycle amplification (RCA) process,[34–36] as described in SI Section S6. Briefly, a circular DNA containing a complementary target sequence was amplified by Phi29 DNA polymerase for 30 min at 30 °C using a primer containing a biotin at the 5′ end. Amplification was stopped by heating the enzyme at 65 °C for 20 min. This resulted in a long ssDNA containing a tandem repeat of the target sequence. Then, with the help of a terminal deoxynucleotidyl transferase (TdT), digoxigenin-dUTP was added to its 3′ end at 37 °C for 2 h followed by heat deactivation at 75 °C for 20 min. Biotin and digoxigenin facilitated tethering of the ssDNA constructs to the optically trapped beads.

Synthesis of Single-Molecule ssRNA Constructs.

The ssRNA templates were synthesized by the rolling cycle transcription (RCT) process,[34,37] which is described in SI Section S7. The synthesis of an ssRNA construct consists of three key steps: (a) synthesis of a long 5′ biotin-RNA construct, (b) synthesis of a short 3′ dig-DNA, and (c) ligation of the 5′ biotin-RNA and 3′ dig-DNA.

To prepare the 5′ biotin-RNA, first, a circular ssDNA was transcribed using T7 RNA polymerase for 3 h at 37 °C. The RCT product was then filtered using a 10K Amicon filter to remove excess NTPs followed by dephosphorylation of the 5′ end using Antarctic phosphatase at 37 °C for 1 h. The 5′ end was then modified with a thio-phosphate using T4 PNK in the presence of ATP(γ)S at 37 °C for 1 h. Biotin maleimide was then linked to the 5′ end of the RCT product via the thiol−maleimide linkage at 65 °C for 30 min. On the other hand, a short ssDNA oligonucleotide was phosphorylated at the 5′ end using T4 PNK followed by the 3′ end modification with dig-dUTP using terminal deoxynucleotidyl transferase (TdT). It was then purified via Amicon filtration, and the 5′ end was adenylated with diphosphate adenine using *m*th RNA ligase by heating at 65 °C for 1 h. The enzyme was heat-deactivated at 85 °C for 5 min. Finally, the 5′ biotin-RNA and the 3′ dig-DNA were ligated by the T4 RNA Ligase 2, truncated KQ (NEB) at 16 °C for 16 h.

Synthesis of a Single-Molecule dsDNA Construct.

A novel strategy was used for the synthesis of a long poly(dA/dT) dsDNA construct, as described in SI Section S8. First, we prepared a long RCA-based poly(dT) whose 5′ end was labeled with biotin. The RCA product was then tailed with dGTP at the 3′ end by TdT at 37 °C for 30 min, which was followed by dig-dUTP labeling at the 3′ end using TdT for 12 h at 37 °C. The enzyme was heat-deactivated at 65 °C for 20 min. Next, a $d(C)_{15}$ oligonucleotide was annealed to the poly(dG) tail of the product at 95 °C for 5 min followed by slow cooling to 25 °C at a rate of −1 °C/min. The $d(C)_{15}$ oligo served as a primer for the extension of a complementary strand to form a dsDNA product by Phi29 DNA polymerase at 30 °C for 30 min. The final dsDNA product had biotin at the 5′ end and digoxigenin at

the 3′ end, which helped to anchor the dsDNA construct between the two optically trapped polystyrene beads in the optical tweezer instrument.

RESULTS AND DISCUSSION

PLL Forms Condensates with Nucleic Acids by LLPS.

To investigate that condensate droplets may form as a result of the liquid−liquid phase separation (LLPS) process, we delivered 4.8 mM each of poly(rU) and PLL via two nanopipets to one of the microfluidic channels filled with 10 mM tris buffer (pH 7.4) supplemented with 100 mM KCl (Figures 1A; see SI Section S4 for nanopipet preparation and Section S5 for nanopipet chamber preparation). As soon as poly(rU) reaches the region downstream of the PLL-containing nanopipet, droplets with submicrometer diameter were formed within seconds at the region close to the pipet opening (Figure 1B,C). Interestingly, when these droplets were escorted by optical traps close to the opening of another nanopipet filled with 1 M NaOH or 0.5 U/μL RNase A, the droplets were dissolved completely within minutes (Figure 1B,D). Since NaOH and RNase A can digest RNA strands,[38,39] these experiments proved that RNA-enriched condensates were indeed a result of LLPS between PLL and poly(rU). Similarly, we also performed bulk phase separation assay for other nucleic acid templates where all nucleic acid−PLL mixtures underwent phase separations (SI Section S11).

Such a microscopy imaging of the microfluidic LLPS process offers several advantages. First, it conserves materials. As few as 50 μL of solution is needed to initiate the LLPS process that can be continuously probed for 10 h. This is especially attractive, as many LLPS processes involve precious protein materials. Second, it has the capability to investigate both the formation and dissolution of the LLPS in real time. Finally, with the help of optical tweezers, this allows us to evaluate the role of a particular component in the LLPS process or reveal the property of a specific condensate droplet.

Single-Molecule Investigation of the PLL−poly(rU) Condensates from Mechanical Perspective.

With the formation of the LLPS droplets confirmed inside the microfluidic device, next, we designed a single-molecule platform in which the conformational change of individual nucleic acid molecules is continuously monitored when PLL is added to initiate LLPS. To this end, two ends of a nucleic acid strand were modified with digoxigenin and biotin, respectively, to facilitate the tethering of the strand to the two optically trapped beads via affinity interactions in a laser tweezer instrument[33] (Figure 2A). Subsequently, by performing a force-ramping procedure of the tethered nucleic acid strand, we compared the elastic behavior of the nucleic acid strand with and without the PLL delivered via a microfluidic channel (see SI Section S3 and Figures S1 and S2).

We first prepared a single-stranded RNA (ssRNA) enriched in uracil (or poly(rU)) by rolling circle transcription (RCT)[34,37] as discussed in Experimental (see details for the synthesis in SI Section S7 and Figure S6), which was followed by chemical modification of biotin at the 5′ end and enzymatic labeling of digoxigenin at the 3′ end. This template was then

tethered between two optically trapped beads, and their force vs extension (FX) profiles were collected with or without PLL in 10 mM tris buffer (pH 7.4) supplemented with 100 mM KCl. Since this poly(rU) template is not expected to have secondary structures,[41] the FX curves with PLL ≤ 0.1 μM did not contain any unfolding features (Figure 2B, state 1). When this tethered template was exposed to 1 μM PLL, the FX curve shifted toward shorter extension (to the left) over time (Figure 2B, state 2), implying that the apparent contour length of the template is shortened. This can be ascribed to the electrostatic attraction between the PLL strands and the poly(rU) template (Figure 2A), which results in the shortening of the RNA template due to the PLL strands serving as staples to bring distal poly(rU) regions closer. As time progressed, the shortening became more obvious, as more PLL strands were associated with the RNA template. The shortening was accelerated upon increasing the PLL concentration to 10 μM (see SI Figure S15 for change in the apparent contour length with increasing PLL concentration). Above this threshold PLL concentration, a new elevated baseline (or plateau) of the FX curve occurred at 9.5 ± 3.3 pN instead of 0 pN force (Figure 2B, state 3). Previously, a similar plateau in FX curves has been attributed to the (de)condensation of the polyamidoamine on the dsDNA strand.[42] Below this concentration, even up to 10 min, we did not observe such an elevated baseline (see SI Figure S15). This clearly indicated the cocondensation of the poly(rU) template and the PLL with a threshold concentration of 10 μM.

The reversible elevated baseline likely indicated a phase transition of the condensation when the poly(rU) is subject to 9.5 pN force. Similar condensation phase transitions have also been observed when condensing agents such as spermidine, hexaamine cobalt(III), or other cationic molecules are used.[42–46] At PLL concentration higher than 30 μM, the condensate became so strong that clean FX curves with very short apparent contour length (Figures 2B and S15, state 4; note the FX curve that shifts to the left) were observed. In fact, at state 4, the condensed assembly was often accompanied by elevated baselines. Under such a high concentration, we surmise that the RNA−PLL condensate matures quickly so that the apparent contour length of the assembly is much reduced. Such a scenario is consistent with the LLPS process in which the phase separation in the form of the droplet formation (Figure 1) occurs in the PLL and nucleic acid mixtures. Occasionally, we observed that the two beads collapsed together upon the addition of 200 μM PLL (SI Figure S8), indicating that the condensation force as a result of the continuous mixing between PLL and poly(rU) exceeds the optical trapping force for the polystyrene beads.

Formation of the Condensates between PLL and Other Nucleic Acids.

Next, we evaluated the mechanical property of different nucleic acid templates in the presence of the PLL in the same buffer (see SI Section S15 and Figures S16–S20). We used DNA strands enriched with adenosine (poly(dA)), thymidine (poly(dT)), poly(dA/dT) duplex, as well as RNA strands enriched with adenosine (poly(rA)). While ssDNA strands were prepared by RCA[35] (see SI Section S6 for details), the synthesis of the ssRNA repeats was achieved with rolling circle transcription as discussed in Experimental (see SI Section S7 for details). For the preparation of poly(dA/dT) duplex DNA, a new procedure was invented (see SI Section S8 for details). Each of these constructs was then attached to two

optically trapped beads to perform force-ramping experiments as shown in Figures 2A and S2.

After comparing FX curves of different PLL−nucleic acid mixtures (Figure 3), we found that except for the duplex DNA and poly(rA) in which the collapses of the two optically trapped beads (state 4) were not observed even at high PLL concentrations (up to 70 and 200 μM PLL, respectively), all mixtures experienced the four states similar to those in the PLL−poly(rU) mixture (see Table 1 and Figure S10 for summary).

Due to the relatively high persistent length of dsDNA (~50 nm[47]) with respect to the ssDNA or ssRNA (~1 nm[48]), it is not surprising that more energy is needed to bend duplex DNA to form condensates with PLL ≥30 μM compared to poly(rU) (PLL ≥ 10 μM), poly(dA) (PLL ≥ 10 μM), or poly(dT) (PLL ≥ 30 μM) (see Table 1 and Figure S11; note poly(dT) is easier to enter the next stage, strong CDS, with respect to the duplex DNA). Above this concentration (30 μM), the stretching FX curves of dsDNA often showed sudden jumps in the force ranging from 10 pN to 40 pN (Figure 3, dsDNA, state 3). These stick-release patterns have been ascribed to the release of the polymer PLL from the condensed interactions,[44,45] which may stem from a coiled (or looped) dsDNA conformation associated with PLL in aqueous media.[49] Similar sudden rupture events were also observed in all other constructs (see Figure 3, state 3), suggesting that condensates form in these constructs.

Compared to dsDNA, it is surprising that poly(rA) is more difficult to form condensates (PLL ≥ 30 μM for dsDNA and PLL ≥ 70 μM for poly(rA); see Table 1). It is known that ssDNA or ssRNA is usually more flexible (persistence length of ~1 nm[48]) than dsDNA. However, poly(rA) is structured because of its strong base-stacking interactions[50] after it forms secondary structures such as rA double helices[51,52] or hairpinlike stem-loop structures.[53] We surmise that compared to dsDNA, which may present steric hindrance due to its compact and well-ordered double helices, PLL may fit better to secondary structures in poly(rA) via electrostatic interactions, making the poly(rA)−PLL complex rigid enough not to easily bend into condensate assemblies. Among different single-stranded nucleic acids, base stacking is strongest in adenines (A) and weakest in thymines (T) or uridines (U).[54] This explains the more difficult tendency for poly(rA) to form condensates compared to poly(dT) or poly(rU) (Table 1 and Figure S11). A similar observation has been observed in bulk experiments in which poly(dA) showed a more difficult tendency to form LLPS droplets compared to poly(dT).[24]

Compared between poly(dA) and poly(rA), NMR studies of homoadenosine polymers showed A-type helix conformation in ssRNA and B-type helix conformation in ssDNA.[55] The different helical geometries[56] therefore suggest that the base-stacking density in single-stranded poly(rA) is more than that in single-stranded poly(dA), causing more rigid structure of poly(rA) with respect to poly(dA), which explains the trend that poly(rA) is more difficult to form condensates than poly(dA) in the presence of PLL.

All these observations prompted us to hypothesize that the condensation process is influenced by the rigidity of the PLL−nucleic acid complex, in which secondary structures of nucleic acid templates may play a critical role.[24] To test this hypothesis, we synthesized

an ssDNA template that contains multiple repeats of human telomeric G-quadruplex (GQ) forming a sequence (5′-TTAGGGTTAGGGTTAGGGTTAGGG-3′) using RCA strategy (detailed synthesis of this template has been described elsewhere[57]). G-quadruplex is a noncanonical DNA structure formed in the G-rich sequences enriched in the regulatory regions of human genomes. Previous studies have shown that GQ forming sequence can form condensates with PLL.[21] When we performed mechanical stretching experiments on the GQ-containing construct as described in Figure 2, we observed hysteresis between extending and relaxing FX curves at PLL concentrations <200 μM (Figure 3E), indicating the formation of GQs in the construct.[57,58] At higher PLL concentrations, however, the hysteresis significantly reduced (see states 2 → 3 in Figure 3E), suggesting that either fewer G-quadruplexes were formed or G-quadruplexes were too strong to unfold up to 50 pN. Given that the apparent contour length of these FX curves is reduced (note the FX curves shift to the left in Figure 3E), it is more likely that G-quadruplexes are too strong to unfold, probably due to the strong electrostatic attraction between the negatively charged phosphate backbone in GQs and the positively charged PLL strands, making the PLL−GQ complex rigid.[21,59] Consistent with the reduction of the hysteresis in the FX curves, we also observed that the GQ construct became harder to form condensates in the presence of PLL as high as 200 μM (see Table 1, Figure S11, and FX curves in Figure 3E; note the state 4 FX curve with much shorter apparent contour length was not observed even at 200 μM PLL). Therefore, we conclude that the electrostatic interaction facilitates the complexation between PLL and different GQ units. Due to the four-stranded DNA backbone in each GQ, the charge density of the poly(GQ) strand is higher than other nucleic acid templates, making it easier to form rigid GQ−PLL complexes, thereby decreasing the tendency to form condensates.

The trend of single-molecule condensation processes for different nucleic acids has also been confirmed by LLPS assays performed in bulk (SI Section S11 and Figure S9). In a mixture of 4.8 mM PLL and 4.8 mM nucleic acids, poly(GQ) and dsDNA formed irregularly shaped droplets, suggesting their solid-like nature. Consistent with this, we found that even freshly prepared droplets from these two nucleic acid templates did not fuse within 5 min (Figure S10 and Table S2). For the rest of the nucleic acid templates, droplets are spherical, suggesting their liquid-like nature. Indeed, the fusion of droplets made of poly(rU)/PLL, poly(dT)/PLL, and poly-(dA)/PLL occurred immediately (<0.3 s) even after 30 min of aging time. However, the fusion between two poly(rA)/PLL droplets did not complete until after 10 s, suggesting that the property of these droplets stays between liquid-like and solid-like. In general, this trend is consistent with that observed in single-molecule experiments in which dsDNA, poly(rA), and poly(GQ) are more difficult to assume condensed conformation within each nucleic acid strand. As a result, there is more chance for these species to interact with other nucleic acid strands intermolecularly (which often occurs in bulk solution), due to their relatively more extended conformation. Persistence length measured from the FX curves by the worm-like-chain model fitting (see state 3 in SI Figures S12 and S14, which contains the force plateau indicative of condensation formation) confirmed that dsDNA, poly(rA), and poly(GQ) have overall longer persistence length compared to poly(dA), poly(dT), or poly(rU), which tends to form condensates (state 3) more easily.

We also fixed the nucleic acid concentration at 4.8 mM and reduced PLL from 4.8 to 0.2 mM. We observed negligible droplet formation in nucleic acid/PLL mixtures (see Figure S9). Since this 0.2 mM PLL was the highest concentration used in the single-molecule experiments, we expect even less phase separation/droplet formation should occur at other PLL concentrations used in the optical-tweezer experiments. These results therefore confirmed that the intermolecular interaction between nucleic acid strands mediated by PLL was a major factor contributing to the phase separation observed in bulk. Since no free nucleic acid strand existed in the solution in optical tweezer experiments, the four-state transitions (Figures 2 and 3) observed in the single-molecule assay are purely intramolecular (with respect to the nucleic acid strand) in nature, which represents a unique perspective to understand the LLPS process.

CONCLUSIONS

In summary, with a highly sensitive single-molecule assay, we were able to dissect the condensate formation between PLL and nucleic acid templates into four different stages within each nucleic acid strand. We have observed that, compared to single-stranded nucleic acid templates, it becomes more difficult for the condensate to form between PLL and duplex DNA. Surprisingly, we have found that poly(rA), due to its propensity to form secondary structures of stacked riboadenosine residues, is even more difficult to form condensates with respect to dsDNA. The adverse effect of rigid nucleic acid secondary structures on the LLPS condensate formation has been confirmed as an ssDNA template hosting rigid G-quadruplexes does not show a strong condensation state with 200 μM PLL. Given the wide occurrence of various secondary nucleic acid structures in cells, such a result suggests a potential biological or synthetic modulation of the LLPS process, for example, by using ligands that can strengthen or weaken the rigidity of nucleic acid structures.

Supplementary Material

Refer to Web version on PubMed Central for supplementary material.

ACKNOWLEDGMENTS

H.M. thanks NIH (R01 CA236350) and NSF (CBET1904921) for financial support.

REFERENCES

(1). Hyman AA; Weber CA; Jülicher F Liquid-Liquid Phase Separation in Biology. Annu. Rev. Cell Dev. Biol 2014, 30, 39–58. [PubMed: 25288112]

(2). Shin Y; Brangwynne CP Liquid phase condensation in cell physiology and disease. Science 2017, 357, No. eaaf4382.

(3). Lyon AS; Peeples WB; Rosen MK A framework for understanding the functions of biomolecular condensates across scales. Nat. Rev. Mol. Cell Biol 2021, 22, 215–235. [PubMed: 33169001]

(4). Banani SF; Lee HO; Hyman AA; Rosen MK Biomolecular condensates: organizers of cellular biochemistry. Nat. Rev. Mol. Cell Biol 2017, 18, 285–298. [PubMed: 28225081]

(5). Gibson BA; Doolittle LK; Schneider MWG; Jensen LE; Gamarra N; Henry L; Gerlich DW; Redding S; Rosen MK Organization of Chromatin by Intrinsic and Regulated Phase Separation. Cell 2019, 179, 470–484.e21. [PubMed: 31543265]

(6). Shakya A; Park S; Rana N; King JT Liquid-Liquid Phase Separation of Histone Proteins in Cells: Role in Chromatin Organization. Biophys. J 2020, 118, 753–764. [PubMed: 31952807]

(7). Peng L; Li E-M; Xu L-Y From start to end: Phase separation and transcriptional regulation. Biochim. Biophys. Acta, Gene Regul. Mech 2020, 1863, 194641. [PubMed: 33017669]

(8). Pessina F; Gioia U; Brandi O; Farina S; Ceccon M; Francia S; d'Adda di Fagagna F DNA Damage Triggers a New Phase in Neurodegeneration. Trends Genet. 2021, 37, 337–354. [PubMed: 33020022]

(9). Oshidari R; Huang R; Medghalchi M; Tse EYW; Ashgriz N; Lee HO; Wyatt H; Mekhail K DNA repair by Rad52 liquid droplets. Nat. Commun 2020, 11, No. 695.

(10). Li P; Banjade S; Cheng H-C; Kim S; Chen B; Guo L; Llaguno M; Hollingsworth JV; King DS; Banani SF; Russo PS; Jiang Q-X; Nixon BT; Rosen MK Phase transitions in the assembly of multivalent signalling proteins. Nature 2012, 483, 336–340. [PubMed: 22398450]

(11). Banjade S; Rosen MK Phase transitions of multivalent proteins can promote clustering of membrane receptors. eLife 2014, 3, No. e04123.

(12). Xiao Q; McAtee CK; Su X Phase separation in immune signalling. Nat. Rev. Immunol 2022, 22, 188–199. [PubMed: 34230650]

(13). Du M; Ea C-K; Fang Y; Chen ZJ Liquid phase separation of NEMO induced by polyubiquitin chains activates NF-κB. Mol. Cell 2022, 82 (13), 2415–2426. [PubMed: 35477005]

(14). Larson AG; Elnatan D; Keenen MM; Trnka MJ; Johnston JB; Burlingame AL; Agard DA; Redding S; Narlikar GJ Liquid droplet formation by HP1α suggests a role for phase separation in heterochromatin. Nature 2017, 547, 236–240. [PubMed: 28636604]

(15). Zhou H; Song Z; Zhong S; Zuo L; Qi Z; Qu L-J; Lai L Mechanism of DNA-Induced Phase Separation for Transcriptional Repressor VRN1. Angew. Chem., Int. Ed 2019, 58, 4858–4862.

(16). Vieregg JR; Lueckheide M; Marciel AB; Leon L; Bologna AJ; Rivera JR; Tirrell MV Oligonucleotide−Peptide Complexes: Phase Control by Hybridization. J. Am. Chem. Soc 2018, 140, 1632–1638. [PubMed: 29314832]

(17). Fay MM; Anderson PJ The Role of RNA in Biological Phase Separations. J. Mol. Biol 2018, 430, 4685–4701. [PubMed: 29753780]

(18). Garcia-Jove Navarro M; Kashida S; Chouaib R; Souquere S; Pierron G; Weil D; Gueroui Z RNA is a critical element for the sizing and the composition of phase-separated RNA−protein condensates. Nat. Commun 2019, 10, No. 3230.

(19). Lin Y; Protter; David SW; Rosen; Michael K; Parker R Formation and Maturation of Phase-Separated Liquid Droplets by RNA-Binding Proteins. Mol. Cell 2015, 60, 208–219. [PubMed: 26412307]

(20). Ukmar-Godec T; Hutten S; Grieshop MP; Rezaei-Ghaleh N; Cima-Omori M-S; Biernat J; Mandelkow E; Söding J; Dormann D; Zweckstetter M Lysine/RNA-interactions drive and regulate biomolecular condensation. Nat. Commun 2019, 10, No. 2909.

(21). Guo W; Ji D; Kinghorn AB; Chen F; Pan Y; Li X; Li Q; Huck WTS; Kwok CK; Shum HC Tuning Material States and Functionalities of G-Quadruplex-Modulated RNA-Peptide Condensates. J. Am. Chem. Soc 2023, 145, 2375–2385. [PubMed: 36689740]

(22). Roden C; Gladfelter AS RNA contributions to the form and function of biomolecular condensates. Nat. Rev. Mol. Cell Biol 2021, 22, 183–195. [PubMed: 32632317]

(23). Jonchhe S; Pan W; Pokhrel P; Mao H Small Molecules Modulate Liquid-to-Solid Transitions in Phase-Separated Tau Condensates. Angew. Chem., Int. Ed 2022, 61, No. e202113156.

(24). Shakya A; King JT DNA Local-Flexibility-Dependent Assembly of Phase-Separated Liquid Droplets. Biophys. J 2018, 115, 1840–1847. [PubMed: 30342746]

(25). Guo Q; Zou G; Qian X; Chen S; Gao H; Yu J Hydrogen-bonds mediate liquid-liquid phase separation of mussel derived adhesive peptides. Nat. Commun 2022, 13, No. 5771.

(26). Deepankumar K; Guo Q; Mohanram H; Lim J; Mu Y; Pervushin K; Yu J; Miserez A Liquid−Liquid Phase Separation of the Green Mussel Adhesive Protein Pvfp-5 is Regulated by the Post-Translated Dopa Amino Acid. Adv. Mater 2022, 34, 2103828.

(27). Hwang DS; Zeng H; Srivastava A; Krogstad DV; Tirrell M; Israelachvili JN; Waite JH Viscosity and interfacial properties in a mussel-inspired adhesive coacervate. Soft Matter 2010, 6, 3232–3236. [PubMed: 21544267]

(28). Cai H; Gabryelczyk B; Manimekalai MSS; Grüber G; Salentinig S; Miserez A Self-coacervation of modular squid beak proteins − a comparative study. Soft Matter 2017, 13, 7740–7752. [PubMed: 29043368]

(29). Liu X; Liu X; Wang H; Dou Z; Ruan K; Hill DL; Li L; Shi Y; Yao X Phase separation drives decision making in cell division. J. Biol. Chem 2020, 295, 13419–13431. [PubMed: 32699013]

(30). Zhang Y; Wei H; Wen W Phase Separation and Mechanical Forces in Regulating Asymmetric Cell Division of Neural Stem Cells. Int. J. Mol. Sci 2021, 22 (19), 10267. [PubMed: 34638607]

(31). Zhao YG; Zhang H Phase Separation in Membrane Biology: The Interplay between Membrane-Bound Organelles and Membraneless Condensates. Dev Cell 2020, 55, 30–44. [PubMed: 32726575]

(32). Davis LK; Ford IJ; Hoogenboom BW Crowding-induced phase separation of nuclear transport receptors in FG nucleoporin assemblies. eLife 2022, 11, No. e72627.

(33). Mao H; Luchette P An integrated laser-tweezers instrument for microanalysis of individual protein aggregates. Sens. Actuators, B 2008, 129, 764–771.

(34). Mohsen MG; Kool ET The Discovery of Rolling Circle Amplification and Rolling Circle Transcription. Acc. Chem. Res 2016, 49, 2540–2550. [PubMed: 27797171]

(35). Ali MM; Li F; Zhang Z; Zhang K; Kang D-K; Ankrum JA; Le XC; Zhao W Rolling circle amplification: a versatile tool for chemical biology, materials science and medicine. Chem. Soc. Rev 2014, 43, 3324–3341. [PubMed: 24643375]

(36). Liu D; Daubendiek SL; Zillman MA; Ryan K; Kool ET Rolling Circle DNA Synthesis: Small Circular Oligonucleotides as Efficient Templates for DNA Polymerases. J. Am. Chem. Soc 1996, 118, 1587–1594. [PubMed: 20830216]

(37). Daubendiek SL; Ryan K; Kool ET Rolling-Circle RNA Synthesis: Circular Oligonucleotides as Efficient Substrates for T7 RNA Polymerase. J. Am. Chem. Soc 1995, 117, 7818–7819. [PubMed: 27524830]

(38). Bernhardt HS; Tate WP Primordial soup or vinaigrette: did the RNA world evolve at acidic pH? Biol. Direct 2012, 7, 4. [PubMed: 22264281]

(39). Haupenthal J; Baehr C; Kiermayer S; Zeuzem S; Piiper A Inhibition of RNAse A family enzymes prevents degradation and loss of silencing activity of siRNAs in serum. Biochem. Pharmacol 2006, 71, 702–710. [PubMed: 16376306]

(40). Schneider CA; Rasband WS; Eliceiri KW NIH Image to ImageJ: 25 years of image analysis. Nat. Methods 2012, 9, 671–675. [PubMed: 22930834]

(41). Richards EG; Flessel CP; Fresco JR Polynucleotides. VI. Molecular properties and conformation of polyribouridylic acid. Biopolymers 1963, 1, 431–446.

(42). Ritort F; Mihardja S; Smith SB; Bustamante C Condensation Transition in DNA-Polyaminoamide Dendrimer Fibers Studied Using Optical Tweezers. Phys. Rev. Lett 2006, 96, No. 118301.

(43). van den Broek B; Noom MC; van Mameren J; Battle C; MacKintosh FC; Wuite GJL Visualizing the Formation and Collapse of DNA Toroids. Biophys. J 2010, 98, 1902–1910. [PubMed: 20441754]

(44). Baumann CG; Bloomfield VA; Smith SB; Bustamante C; Wang MD; Block SM Stretching of Single Collapsed DNA Molecules. Biophys. J 2000, 78, 1965–1978. [PubMed: 10733975]

(45). Murayama Y; Sakamaki Y; Sano M Elastic Response of Single DNA Molecules Exhibits a Reentrant Collapsing Transition. Phys. Rev. Lett 2003, 90, No. 018102.

(46). Hormeño S; Moreno-Herrero F; Ibarra B; Carrascosa JL; Valpuesta JM; Arias-Gonzalez JR Condensation prevails over B-A transition in the structure of DNA at low humidity. Biophys. J 2011, 100, 2006–2015. [PubMed: 21504737]

(47). Baumann CG; Smith SB; Bloomfield VA; Bustamante C Ionic effects on the elasticity of single DNA molecules. Proc. Natl. Acad. Sci. U.S.A 1997, 94, 6185–6190. [PubMed: 9177192]

(48). Smith SB; Cui Y; Bustamante C Overstretching B-DNA: The Elastic Response of Individual Double-Stranded and Single-Stranded DNA Molecules. Science 1996, 271, 795–799. [PubMed: 8628994]

(49). Shukla RS; Qin B; Cheng K Peptides Used in the Delivery of Small Noncoding RNA. Mol. Pharmaceutics 2014, 11, 3395–3408.

(50). Friedman RA; Honig B A free energy analysis of nucleic acid base stacking in aqueous solution. Biophys. J 1995, 69, 1528–1535. [PubMed: 8534823]

(51). Gleghorn ML; Zhao J; Turner DH; Maquat LE Crystal structure of a poly(rA) staggered zipper at acidic pH: evidence that adenine N1 protonation mediates parallel double helix formation. Nucleic Acids Res. 2016, 44, 8417–8424. [PubMed: 27288442]

(52). Tang TTL; Passmore LA Recognition of Poly(A) RNA through Its Intrinsic Helical Structure. Cold Spring Harbor Symp. Quant. Biol 2019, 84, 21–30. [PubMed: 32295929]

(53). Moqtaderi Z; Geisberg JV; Struhl K Secondary structures involving the poly(A) tail and other 3′ sequences are major determinants of mRNA isoform stability in yeast. Microb Cell 2014, 1, 137–139. [PubMed: 25279376]

(54). Buhot A; Halperin A Effects of stacking on the configurations and elasticity of single-stranded nucleic acids. Phys. Rev. E 2004, 70, No. 020902.

(55). Isaksson J; Acharya S; Barman J; Cheruku P; Chattopadhyaya J Single-Stranded Adenine-Rich DNA and RNA Retain Structural Characteristics of Their Respective Double-Stranded Conformations and Show Directional Differences in Stacking Pattern. Biochemistry 2004, 43, 15996–16010. [PubMed: 15609994]

(56). Pierce BA Genetics: A Conceptual Approach; Macmillan, 2012.

(57). Pokhrel P; Wang J; Selvam S; Jonchhe S; Mandal S; Mao H Ensemble Force Spectroscopy of a G-Quadruplex Cluster on a Single-Molecule Platform. Biomacromolecules 2022, 23, 4795–4803. [PubMed: 36322676]

(58). Chowdhury S; Wang J; Nuccio SP; Mao H; Di Antonio M Short LNA-modified oligonucleotide probes as efficient disruptors of DNA G-quadruplexes. Nucleic Acids Res. 2022, 50, 7247–7259. [PubMed: 35801856]

(59). Mimura M; Tomita S; Shinkai Y; Hosokai T; Kumeta H; Saio T; Shiraki K; Kurita R Quadruplex Folding Promotes the Condensation of Linker Histones and DNAs via Liquid−Liquid Phase Separation. J. Am. Chem. Soc 2021, 143, 9849–9857. [PubMed: 34152774]

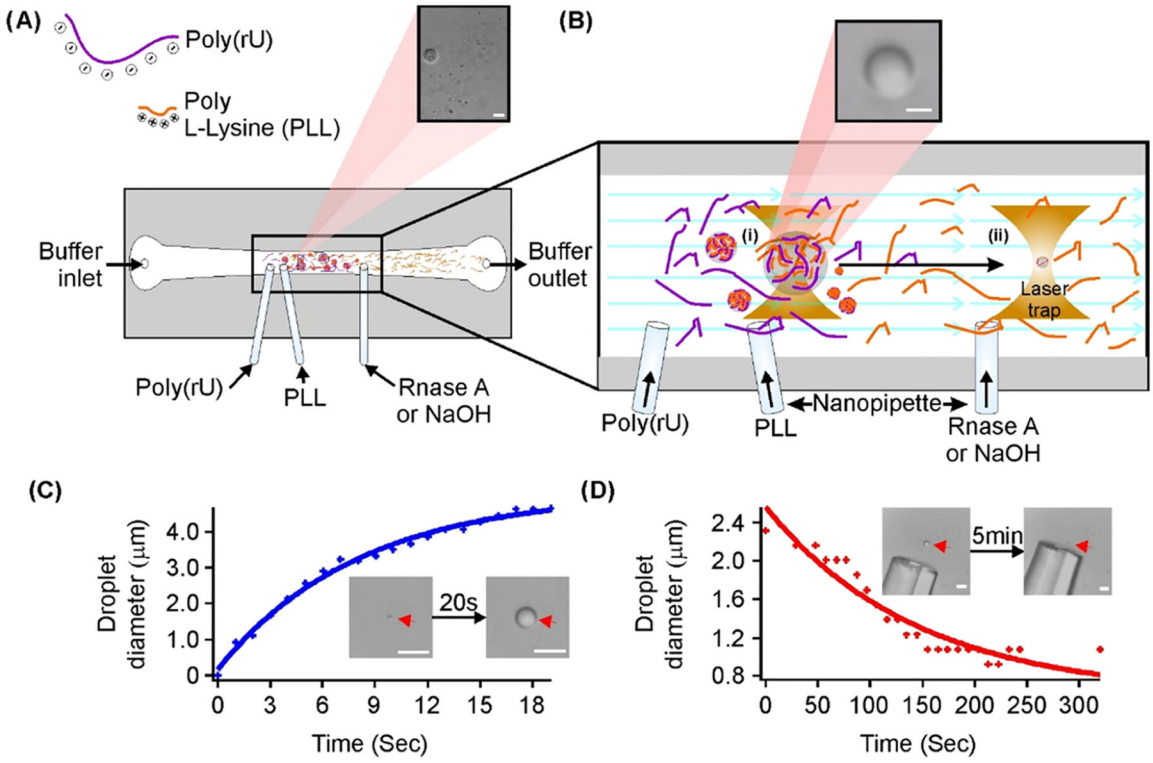

Figure 1.

Schematic of the microfluidic chamber to observe the formation and dissolution of PLL (30−70 kDa) (gold) and poly(rU) (100−600 kDa) nucleic acid (purple) condensates (A). The chamber consists of a microchannel where three nanopipets are placed for the delivery of nucleic acids, PLL, and a destabilizing agent separately. (B) The blowup image of the region around the three nanopipets. Phase-separated condensate droplets form close to the opening of the PLL-containing nanopipet where PLL and poly(rU) mix. The droplet was then trapped using optical tweezers (i) and moved to region ii downstream of a destabilizing agent (RNase A or NaOH). (C) Formation kinetics of a condensate upstream of a destabilizing agent and (D) dissolution kinetics of the droplet downstream of the destabilizing agent. Video of droplet formation and dissolution was recorded. The video frames were converted to images, which were then analyzed using the image analysis software, ImageJ,[40] to measure the droplet diameter. Scale bar: 5 μm.

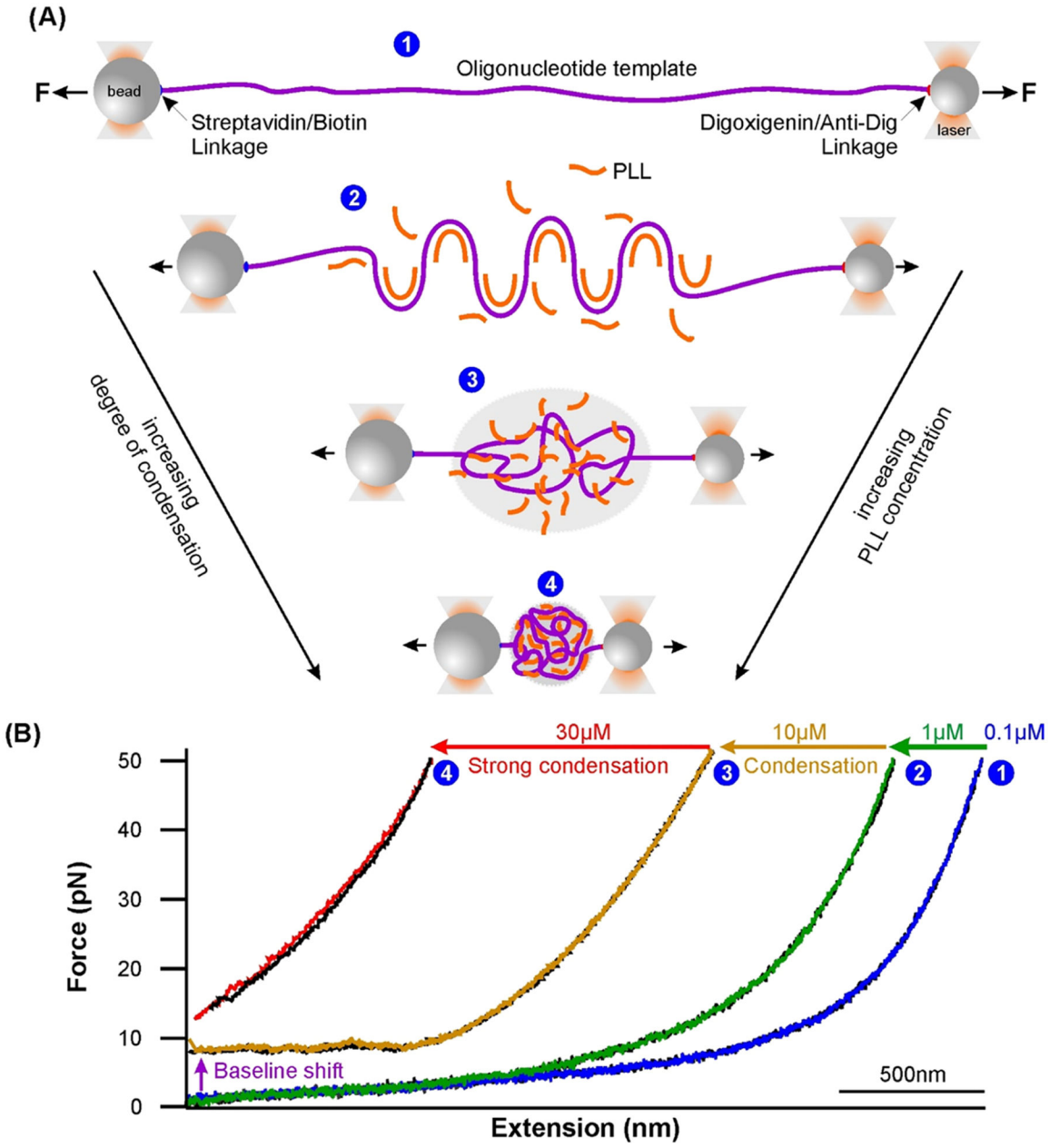

Figure 2.

(A) Schematic of the optical tweezer setup to monitor the tension of nucleic acid templates in the presence of PLL. A nucleic acid template tethered between a pair of beads is stretched or relaxed by moving one of the optically trapped beads. (B) Typical force−extension curves after stretching and relaxing poly(rU) with different PLL concentrations. In the absence of PLL or very low PLL concentration (≤1 μM), the template shows FX curves without unfolding features that are indicative of folded structures (state 1). At low PLL concentrations (>1 μM), the interaction between PLL and the nucleic acid template slightly reduces the apparent contour length of the template (state 2, FX curve shifts to the left). With further increase in PLL concentration, the baseline shifts up to show a plateau in the

FX curve, which indicates the condensation process (state 3), while the magnitude of the force plateau suggests the critical mechanical force to disrupt a condensed phase. At even higher PLL concentrations, the apparent contour length of the tether is significantly reduced, consistent with a much-condensed state (state 4).

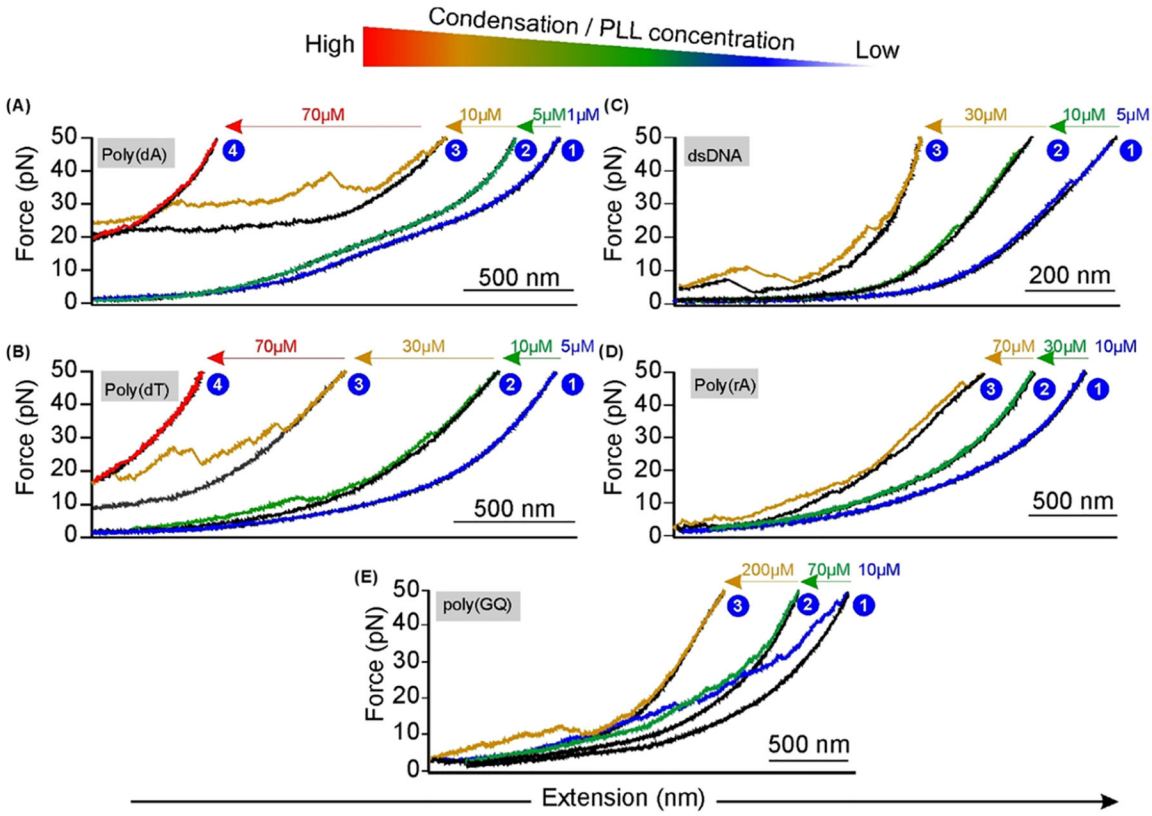

Figure 3.

Typical force−extension (FX) curves (stretching: colored; relaxing: black) representing different stages of the PLL−nucleic acid condensates.

Table 1.

Transition Conditions of the Condensates Formed between PLL and Single-Molecule Nucleic Acid Templates[a]

	templates					
[PLL] (μM)	**Poly(rU)**	**Poly(dA)**	**Poly(dT)**	**ds poly(dA/dT)**	**Poly(rA)**	**Poly(GQ)**
0.1	no CDS/No BLS (6)					
1	curve shortening (4)	no CDS/No BLS (7)				
5	curve shortening (5)	curve shortening (6)	no CDS/No BLS (4)	no CDS/No BLS (6)		
10	CDS/BLS (7)	CDS/BLS (3)	curve shortening (4)	curve shortening (5)	no CDS/No BLS (8)	no CDS/No BLS (6)
30	strong CDS (6)	CDS/BLS (6)	CDS/BLS (6)	CDS/BLS (4)	curve shortening (5)	curve shortening (4)
70		strong CDS (5)	strong CDS (8)	CDS/BLS (6)	CDS/BLS (4)	curve shortening (3)
200				CDS/BLS (3)	CDS/BLS (5)	CDS/BLS (6)

[a]The numbers in parentheses represent the number of molecules investigated. CDS, condensation; BLS, baseline shift (i.e., force plateau).